

Dyson orbitals of N₂O: Electron momentum spectroscopy and symmetry adapted cluster-configuration interaction calculations

Y. R. Miao, C. G. Ning,^{a)} K. Liu, and J. K. Deng^{b)}

Department of Physics, State Key Laboratory of Low-Dimensional Quantum Physics, Tsinghua University, Beijing 100084, People's Republic of China

(Received 25 February 2011; accepted 4 May 2011; published online 26 May 2011)

Electron momentum spectroscopy and symmetry adapted cluster-configuration interaction (SAC-CI) theory were combined to study electron correlation effects in nitrous oxide molecule (N₂O). The SAC-CI General-R method accurately reproduced the experimental ionization spectrum. This benchmarked method was also introduced for calculating the momentum distributions of N₂O Dyson orbitals. Several calculated momentum distributions with different theoretical methods were compared with the high resolution experimental results. In the outer-valence region, Hartree-Fock (HF), density functional theory (DFT), and SAC-CI theory can well describe the experimental momentum distributions. SAC-CI presented a best performance among them. In the inner-valence region, HF and DFT cannot work well due to the severe breaking of the molecular orbital picture, while SAC-CI still produced an excellent description of experimental momentum profiles because it can accurately take into account electron correlations. Moreover, the thermally averaged calculation showed that the geometrical changes induced by the vibration at room temperature have no noticeable effects on momentum distribution of valence orbitals of N₂O. © 2011 American Institute of Physics. [doi:10.1063/1.3593271]

I. INTRODUCTION

Electronic structures of atoms and molecules are of particular interest for chemists and a key factor in understanding chemical properties. Electron momentum spectroscopy, which is based on a kinetic-complete (*e*, 2*e*) ionization experiment, can directly measure binding energies and momentum distributions of individual molecular orbitals at the same time.^{1,2} To interpret the experimental results, the frozen orbital approximation has been widely used in electron momentum spectroscopy (EMS) field.³ In combination with Hartree-Fock (HF) or density functional theory (DFT) calculations,⁴⁻⁶ it can provide a good description of some experimental results. However, the frozen orbital approximation is not accurate enough if the electron correlation is very strong in some molecular system. Recently, some high level calculations, such as configure interaction⁷ and Green's function methods,⁸ have been used to interpret the experimental results. They can reproduce the experimental results for the outer valence orbitals very well through including the electron correlation. But for the inner valence regions, even higher orders of electron excitations are required to reproduce the complicated satellite lines.⁹ The symmetry adapted cluster-configuration interaction (SAC-CI) method, which can include the electron correlation up to sextuple, has produced very impressive results in the inner valence regions.^{10,11} Although SAC-CI has been used to interpret binding energy spectra, there is no report on using SAC-CI to calculate the momentum distributions, which is the most important feature of EMS.

^{a)}Electronic mail: ningcg@tsinghua.edu.cn.

^{b)}Electronic mail: dj-k-dmp@tsinghua.edu.cn.

In present work, we reported the theoretical momentum distributions of N₂O molecule by SAC-CI method. N₂O is of great importance in chemistry and atmospheric science, and also an important prototype molecule for theoretical and experimental works.¹²⁻²⁶ The valence binding energy spectra of N₂O have been previously investigated using photoelectron spectroscopy with the synchrotron radiation,²⁷ x ray,²⁸ and dipole (*e*, 2*e*) techniques.²⁹ Ehara *et al.* have intensively studied the satellite structure of N₂O ionization energy spectra by SAC-CI method.³⁰ The EMS experimental results of N₂O have also been previously reported.³¹⁻³³ However, there is no detailed theoretical explanation for the experimental momentum distributions of those N₂O satellite structures.

The experiment was performed on our third-generation high resolution and high efficiency electron momentum spectrometer. The SAC-CI calculations are in excellent agreement with the experimental results for both the binding energy spectrum and the momentum distributions. HF, DFT, and outer valence green function (OVGF) (Refs. 34 and 35) calculations were also presented.

II. THEORETICAL AND EXPERIMENTAL RESULTS

A. Experimental methods and basic theories of EMS

The descriptions and operations of our high resolution EMS spectrometer have been reported in details previously.^{36,37} Only a brief description is given here. Our spectrometer takes the symmetric non-coplanar scattering geometry. A double-toroidal energy analyzer is used for analyzing the energies and angles of electrons. At the end of the trajectory of electron, two large position sensitive detectors are used to determine the positions of electrons accurately. With

this arrangement, we can significantly increase the collecting efficiency of the coincidental (e, 2e) events.

In present experiment, the barium oxide cathode electron gun is employed to generate an electron beam with a low energy spread and a low divergence angle due to the low working temperature (1100 K). The coincidental instrumental energy resolution is 0.68 eV (full width at half maximum, FWHM), which was obtained through the calibration of Ar sample. The finite spectrometer acceptance angle of θ is $\pm 0.84^\circ$ (one standard deviation), and the angle resolution of azimuthal angle φ is $\pm 0.53^\circ$ (one standard deviation). The gaseous sample of N₂O with a purity of 99.99% was used and the flow rate was controlled by a needle valve. No impurities were observed the binding energy spectrum.

Under the symmetric non-coplanar geometry, the momentum of electrons in atoms and molecules before the reaction can be obtained through the out-of-plane azimuthal angle φ between the two knocked-out electrons using the equation

$$p = \sqrt{(2p_1 \cos \theta_1 - p_0)^2 + (2p_1 \sin \theta_1 \sin(\varphi/2))^2}, \quad (1)$$

where p_0 and p_1 , respectively, represent the momentum of the incident electron and the outgoing electron. The (e, 2e) ionization cross section is directly related to Dyson orbital,^{1,38-41} defined as the overlap of the initial ground state Ψ_g^N and the final state Ψ_f^{N-1} , i.e.,

$$\Phi^{Dyson} = \langle \Psi_f^{N-1} | \Psi_g^N \rangle, \quad (2)$$

where N is the number of electrons. At the high electron impact energies and high momentum transfer, EMS ionization intensities are simply proportional to electronic structure factors obtained as the absolute square of Dyson orbitals in momentum space. In practice, Dyson orbitals are very hard to compute and have commonly been empirically approximated by Hartree-Fock orbitals or Kohn-Sham orbital. Within the plane wave impulsive approximation (PWIA) framework,¹ and the target Hartree-Fock approximation or the target Kohn-Sham approximation,^{42,43} the differential EMS cross section for randomly oriented molecules at gas phase is given by¹

$$\sigma_{EMS} \propto S_i^f \int d\Omega |\psi_i(p)|^2, \quad (3)$$

where S_i^f denotes the spectroscopic factor. S_i^f is particularly important in accounting for the shake-up and shake-off processes due to configuration interactions in the final state. The integral is known as the spherically averaged one-electron momentum distribution.

B. The SAC-CI method and Dyson orbital

The SAC-CI method has been developed by the Nakatsuji laboratory both in theories and algorithms,⁴⁴⁻⁴⁷ and has been successfully applied to various chemical phenomena, especially the ionization potential calculations.^{48,49} Recently, SAC-CI theory was also used to explain the (e, 2e) binding energy spectra of furan, pyrrole, and thiophene.⁵⁰ In present work, SAC-CI method was used to study the momentum distributions in N₂O.

The SAC-CI theory generally requires SAC and SAC-CI calculations. SAC calculates symmetry-adapted cluster ex-

pansion for singlet closed-shell ground state and SAC-CI calculates open-shell singlet excited states, triplet ground and excited states, doublet ionized and doublet electron-attached ground and excited states. SAC calculation is always necessary for SAC-CI calculations. There are two ways contained in SAC-CI to describe the excitations according to the choice of the linked operators, namely, SD-R method and General-R method. Only single and double excitations are contained in SAC-CI SD-R method, while triple and even higher excitations are involved in SAC-CI General-R methods.

The symmetry adapted cluster (SAC) expansion is defined for the totally symmetric singlet closed-shell state as

$$|\psi_g^{SAC}\rangle = \exp\left(\sum_I C_I S_I\right) |0\rangle = \left(1 + \sum_I C_I S_I + \frac{1}{2} \sum_{I,J} C_I C_J S_I S_J + \dots\right) |0\rangle, \quad (4)$$

where $|0\rangle$ is the Hartree-Fock closed-shell determinant and S_I is symmetry adapted excitation operator. The SAC wave function well describes the electron correlation of the ground state. The above cluster expansion is based on the exponential hypothesis. This is mainly due to an approximate separability in the electron correlation. The exponential hypothesis and the commutative operators lead to the size consistency property.^{51,52}

Using the SAC wave function, we can write the SAC-CI wave functions as

$$|\psi_f^{SAC-CI}\rangle = P |\psi_g^{SAC}\rangle. \quad (5)$$

The excitatory P is defined as

$$P = \sum_{K=0}^N d_K R_K. \quad (6)$$

The equations are solved by diagonalizing symmetrized matrices. The variational solution is obtained by applying the variational principle to SAC and SAC-CI wavefunction. Obviously, the wavefunctions of SAC-CI and SAC are mutually orthogonal and Hamiltonian orthogonal.

The SAC-CI combined the merits of size consistency of the cluster expansion and the energy upper boundary of CI. The wavefunctions depend critically on the SAC solutions for the ground state.

Dyson orbital constructed by SAC-CI is the linear combination of orthogonal HF orbitals with required symmetry and finally normalized to a factor called spectroscopic factor, as given by

$$\Phi^{Dyson}(IP) = \langle \Psi_f^{N-1} | \Psi_g^N \rangle = \sum_i c_i \phi_i, \quad (7)$$

$$S_i^f = \sum_i c_i^2, 0 \leq S_i^f \leq 1,$$

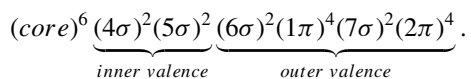
where IP , Ψ_f^{N-1} , Ψ_g^N , ϕ_i , c_i , and S_i^f denote the ionization potential, residual ion state, initial target state, HF orbitals, expanding coefficients, and spectroscopic factors, respectively.

The SAC-CI calculations were executed in GAUSSIAN 03 program.⁵³ The correlated SAC and SAC-CI wavefunctions were used for the ground and final states for including both ground and final states correlations. All information required to construct Dyson orbital was extracted by a home-compiled program. Fourier transformations and the spherical average of momentum distributions for each Dyson orbital were calculated with our *NEMS* program.⁵⁴ The calculated momentum distributions were further compared with the experimental results.

III. RESULTS AND DISCUSSION

A. Binding energy spectra of N₂O

N₂O is a linear molecule, belongs to the C_{∞v} point group. In the ground state, the 18 valence electrons are arranged in six orbitals, including two degenerate orbitals. Its electronic ground state has the following configuration:



The binding energy spectra (BES) of N₂O in the region 10-45 eV were shown in Fig. 1 for the incident energy of 1200 eV. Figure 1(a) shows the x-ray photoelectron spectrum of N₂O. Figure 1(b) is the EMS ionization energy spectrum summed over all azimuthal angles φ . It can be seen that there are four well resolved sharp peaks in the outer valence region and several relative weak peaks in the inner valence region. The experimental BES at each azimuthal angle was fitted by 14 Gaussian functions to obtain the experimental momentum distributions for each peak. The widths of Gaussian functions were combinations of the spectrometer energy resolution and the Frank-Condon widths estimated from the high resolution PES.¹² The simulated ionization spectrum using the SAC-CI General-R method was shown in Fig. 1(c). It can be seen that the simulation can reproduce the most of features of experimental binding energy spectrum.

In outer valence regions (<22 eV), each Dyson orbital has one dominant HF orbital component. The main lines at 12.93, 16.45, 18.30, and 20.17 eV can be considered to be the ionization from 2 π , 7 σ , 1 π , and 6 σ orbitals, respectively. As Fig. 1 shows, the inner orbitals broken up into a bunch of congested satellite lines in the region of 22-42 eV. It is hard to tell which the main lines are, and which satellites are in this region. The concept of molecular orbital in this region is no longer a good picture. So, it is not appropriate to label the experimental peaks using HF orbitals. Table I compared the experimental ionization potentials and spectroscopic factors of these peaks and the calculated values. OVGf method presents reliable results for the outer valence orbitals. With the statistical average of orbital potential method (SAOP),⁵⁵ DFT also produced reasonable results. Only the highest level calculation, SAC-CI General-R method was in excellent agreement with experimental results in both outer valence and inner valence regions. In Table I, the main difference between present results and Ehara *et al.* comes from the selection of R-operators: we included the R-operators up to the quintuple

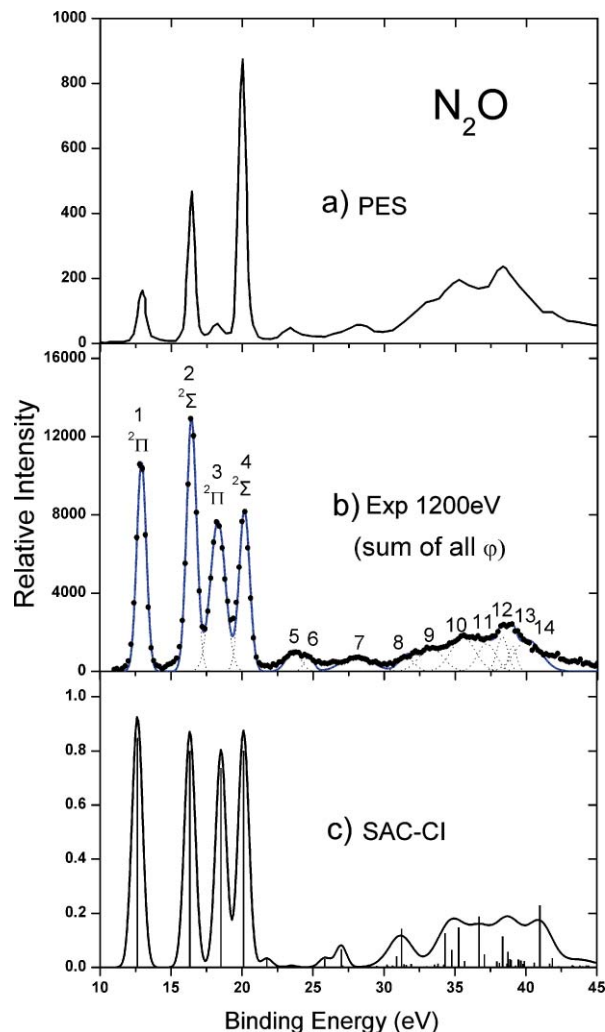


FIG. 1. Binding energy spectra of N₂O. (a) X-ray PES of N₂O measured at photon energy of 1486.6 eV.²⁸ (b) EMS ionization spectra summed over all φ angles, obtained at impact energy of 1200 eV plus binding energies. The dashed lines represent individual fitting Gaussian peaks and the solid line is summation. (c) Simulated ionization spectrum by SAC-CI General-R method. The heights of short spikes represent the spectroscopic factors.

excitation in present work, while Ehara *et al.* included them up to the triple excitation.³⁰

B. Momentum distributions for Dyson orbitals in the outer valence region

In outer valence regions, HF orbitals and DFT KS orbitals are usually good approximations to Dyson orbitals. In Fig. 2, three types of calculated momentum distributions were compared with experimental momentum distributions. For DFT calculations, there are many different types of reported exchange-correlation functional whose performance usually depends on the specific system, and no exchange-correlation functional is omnipotent. Here, three typical functions DFT-B3LYP,^{56,57} DFT-SVWN,^{58,59} and DFT-PBE1PBE (Ref. 60) were compared with each other. The correlated consistent basis set cc-pVTZ (Ref. 61) was employed for all calculations. In general, all calculations can well reproduce the experimental momentum distributions. For peak 1 and peak 3

TABLE I. Ionization potentials (IP) (eV) and spectroscopic factors (SF) of N₂O.

EMS ^a IP(SF)	PES ^b IP	OVSF ^a IP(SF)	SAC-CI ^a (General-R) IP(SF)	SAC-CI ^c (General-R) IP(SF)	SOAP ^a IP
12.93(0.86)	12.89	12.4(0.87)	12.63(0.852) ^d	12.64(0.862) ^d	13.54
16.45(0.82)	16.38	16.0(0.80)	16.32(0.799)	16.27(0.794)	16.65
18.30(0.68)	18.24	18.0(0.84)	18.51(0.743) ^d	18.25(0.629) ^d	18.86
	19.5			19.95(0.093) ^d	
20.17(0.75)	20.11		20.10(0.801)	20.05(0.788)	20.10
	22.6		21.74(0.031) ^d	21.57(0.013) ^d	
23.61(0.16)	24.1		25.83(0.031)	23.95(0.043)	
24.70(0.10)			26.99(0.071) ^d	25.49(0.111) ^d	
28.10(0.23)	28.7		30.20(0.013) ^d	28.34(0.015) ^d	
				28.93(0.045)	
			30.89(0.041)	29.69(0.045)	
			31.24(0.142)	29.85(0.041)	
31.55(0.09)			31.56(0.009)	31.90(0.012) ^d	32.15
			31.92(0.012)	32.66(0.039)	
33.3(0.23)	33.7		33.56(0.014) ^d	33.34(0.022)	
			33.80(0.014)	34.31(0.102)	
			34.30(0.126)	34.85(0.124)	
			34.78(0.064)	35.28(0.110)	
35.55(0.35)			35.26(0.148)	35.62(0.031)	
			35.69(0.024)	35.86(0.018)	
			36.70(0.188)	36.55(0.028)	36.25
37.2(0.18)	37.3		37.07(0.047)	37.08(0.082)	
			37.96(0.022)	37.59(0.052)	
			38.13(0.016)	37.84(0.052)	
38.3(0.12)			38.36(0.114)	38.30(0.234)	
			38.68(0.014)		
			38.72(0.016)		
			38.73(0.057)		
			38.89(0.031)		
39.03(0.11)			38.97(0.027)		
			39.47(0.029)		
			39.62(0.026)	39.68(0.096)	
			39.66(0.025)		
			39.89(0.023)	40.00(0.129)	
			40.59(0.018)	40.22(0.057)	
40.1(0.25)			40.98(0.229)	40.86(0.183)	
			41.86(0.034)	41.79(0.028)	
				41.86(0.015)	

^aThis work. OVSF and SAC-CI calculations were executed in GAUSSIAN 03 program suite (Ref. 53), and SAOP was done in ADF program (Ref. 73).

^bFrom Ref. 28.

^cFrom Ref. 30.

^dDyson orbitals belong to ²Π state, while others belong to ²Σ state.

[Figs. 2(a) and 2(c)], HF, DFT, and SAC-CI predicted almost the same distributions. All calculations underestimated the experimental intensity at low momentum regions ($p < 0.4$ a.u.). The similar unexpected higher intensity at low momentum regions was also observed recently in other molecular orbitals, such as HOMO of O₂ (Ref. 62) and 1b_{3g} of C₂H₄,⁶³ which was ascribed to the distorted wave effects. To test the possibility of the distorted wave effects, the experiment was also conducted under the higher impact energy 2400 eV. As Fig. 2 showed, there were no notable difference between the experimental momentum distributions for 2400 eV and that for 1200 eV. So, the distorted wave effects cannot explain the discrepancy, which is in agreement with previous work by Takahashi *et al.*¹⁶ The further studies are needed to

understand the discrepancy. Vibrational effects will be investigated in the latter section.

For peak 2 and peak 4 [Figs. 2(b) and 2(d)], there are some discernable differences among those methods. HF calculation (curve 1) significantly underestimated the experimental intensity of peak 2 in the low momentum region (Fig. 2(b), $p < 0.5$ a.u.). DFT-B3LYP and DFT-PBE1PBE (curves 2, 4) improved, and SAC-CI and DFT-SVWN (curves 5, 3) were in excellent agreement with the experimental momentum distributions. Interestingly, DFT-SVWN produced the almost same distribution as SAC-CI did for this Dyson orbital. A similar trend was observed for peak 4 in Fig. 2(d) in the momentum region between 0.4 a.u. and 0.8 a.u.: HF underestimated the experimental intensities, and

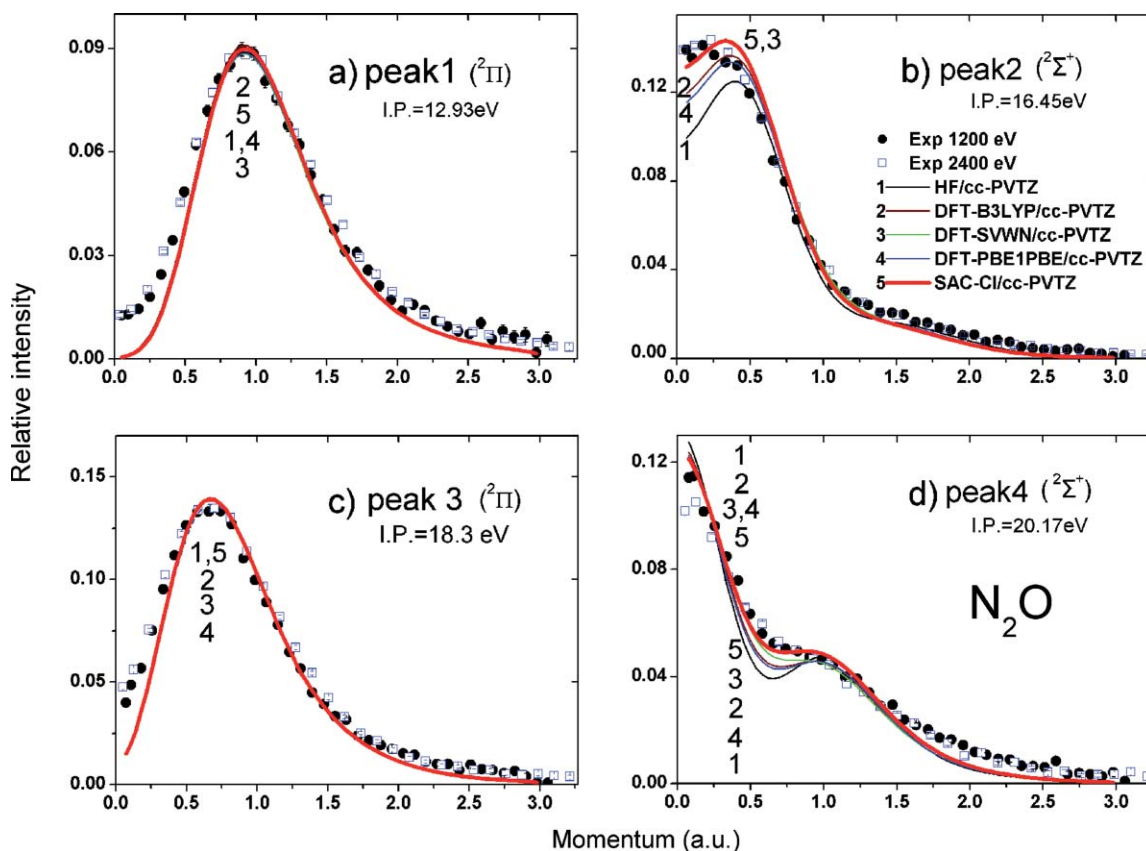


FIG. 2. Spherically averaged momentum distributions of N₂O in the outer valence region of 12–22 eV.

DFT-PBE1PBE, DFT-B3LYP, and DFT-SVWN gradually improved, and SAC-CI fitted best with the experimental distributions. Compared with HF, DFT partly took account of the electron correlation through the exchange-correlation potential. Electron correlations and relaxations during the ionization were more accurately described by SAC-CI General-R method. It is reasonable to conclude that electron correlations play an important role for describing the electron density distributions of N₂O.

It should be noted that there are three significant configurations: $(6\sigma)^{-1}$, $(2\pi)^{-1}(7\sigma)^{-1}(3\pi)^1$, and $(2\pi)^{-1}(7\sigma)^{-1}(4\pi)^1$ for final state at 20.17 eV. In the language of configuration interaction (CI), satellite lines may exhibit itself because of the interaction of the single-hole (1h) configuration with two hole one particle (2h-1p) or even higher excited configurations. Generally, the 2h-1p configuration has higher energy than the 1h configuration in outer valence region. There is one mechanism called one-up-and-one-down, which may induce 2h-1p configurations, as shown in Fig. 3. The Dyson orbital at 20.17 eV includes three relative significant configurations: $-0.893(6\sigma)^{-1} + 0.163(2\pi)^{-1}(7\sigma)^{-1}(3\pi)^1 + 0.152(2\pi)^{-1}(7\sigma)^{-1}(4\pi)^1$.

C. Momentum distributions for Dyson orbitals in the inner valence region

In the inner valence region of N₂O (>22 eV), there are a number of congested satellite lines. To obtain the experimental momentum distributions, ten Gaussian peaks were used to

fit the binding spectrum at this region [Fig. 1(b)]. Since these peaks were not well resolved, they were arranged into four groups for the comparison with theoretical calculations:

- Group I: peak 5, 6;
- Group II: peak 7;
- Group III: peak 8, 9, 10;
- Group IV: peak 11, 12, 13, 14.

Since the HF and DFT method cannot explain satellite lines because of the break up of molecular orbitals, only SAC-CI method was used to calculate their momentum distributions. As shown in Fig. 4, the theoretical momentum distributions using SAC-CI General-R method can well reproduce the experimental profiles.

The peak 5 (23.61 eV) was attributed to $^2\Sigma$ state and peak 6 (24.7 eV) was attributed to $^2\Pi$ state, whose assignment is the same as the dipole (e, 2e) work²⁹ and the SAC-CI calculation by Ehara *et al.*³⁰ Peak 7 (28.1 eV) was related to two $^2\Sigma$ states and one $^2\Pi$ state in Table I. The momentum distribution of peak 7 was well described by the theoretical calculation in Fig. 5(b). Peak 8, peak 9, and peak 10 were mainly attributed to $^2\Sigma$ states. These three peaks were summed up in comparison with the theoretical results in Fig. 4(c). It can be seen that SAC-CI well described the observed results. Peaks 11–14 were all attributed to $^2\Sigma$ states. These assignments were also consistent with Ehara *et al.*³⁰ Momentum spectra of peaks 11–14 were summed up in comparison with the theoretical results in Fig. 4(d). The ionization potentials and spectroscopic factors of these satellites were summarized in Table I.

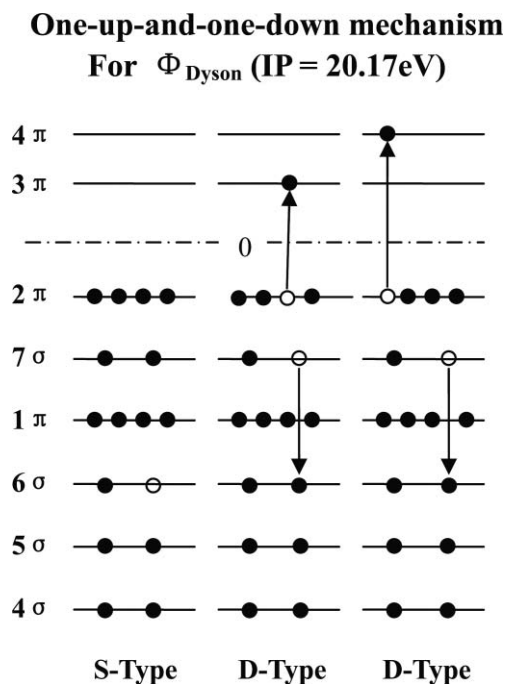


FIG. 3. Schematic of the one-up-and-one-down mechanism for Dyson orbital at 20.17 eV. There are three important configurations, S-Type: $-0.893(6\sigma)^{-1}$, D-Type: $0.163(2\pi)^{-1}(7\sigma)^{-1}(3\pi)^1$, and $0.152(2\pi)^{-1}(7\sigma)^{-1}(4\pi)^1$. The coefficients are obtained by SAC-CI General-R calculations. The plotted energy levels are not in scale.

D. Vibrational effects on momentum distributions

The electron momentum distributions are highly depends on the molecular geometric structure. A floppy molecule easily deviates from its equilibrium structure^{64–69} due to the low frequency vibration at room temperature. Therefore, the thermally averaged momentum distribution may be different

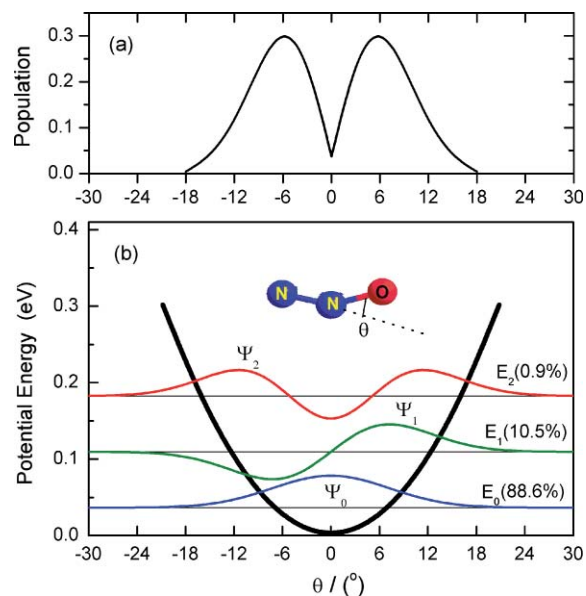


FIG. 5. (a) Population vs the bending angle θ for the vibration of N_2O at room temperature. (b) Potential energy curve (black thick line) and the first three vibrational wave functions of the bending vibrational mode of N_2O . The percentage on each horizontal line represents the population on each energy level at room temperature. The inset shows the bending vibration mode ($\nu = 589 \text{ cm}^{-1}$).

from that of the equilibrium structure. For example, the low frequency vibrational modes notably change the momentum distributions of highest occupied molecular orbital (HOMO) of $\text{W}(\text{CO})_6$.⁷⁰ The thermally averaged momentum distributions, which considered the vibrational effects, can well reproduce the unexpected higher experimental intensity of $\text{W}(\text{CO})_6$ HOMO at the low momentum region. To further understand the unexpected higher intensities for peak 1 and peak 3 of N_2O in Figs. 2(a) and 2(c), the vibrational effects should be

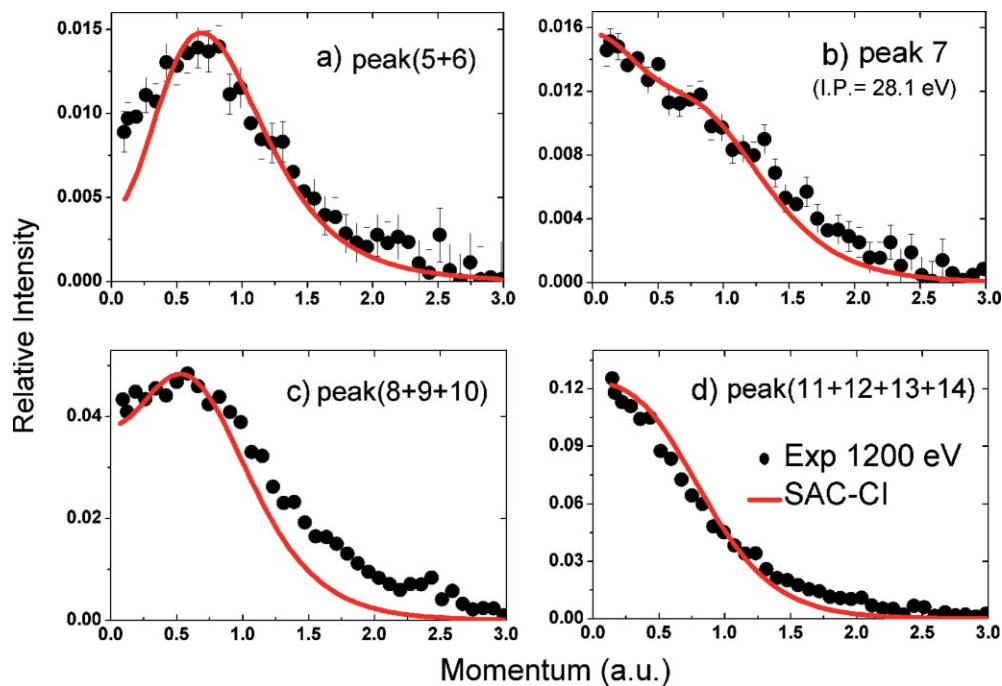


FIG. 4. Spherically averaged momentum distributions of N_2O in the inner valence region of 22–42 eV.

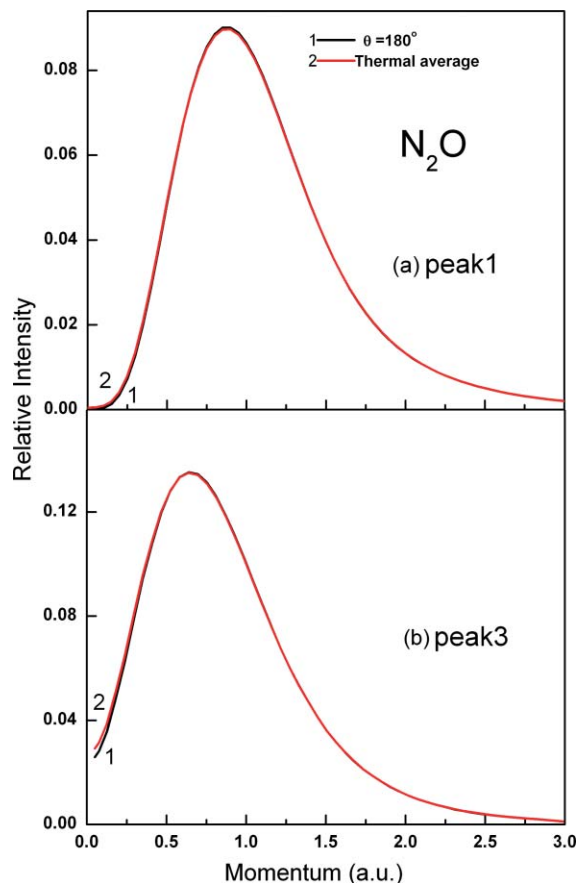


FIG. 6. Spherically and thermally averaged momentum distributions of peak 1 and peak 3 orbitals of N₂O with considering the vibrational effects at room temperature.

considered carefully. The lowest vibrational frequency (589 cm⁻¹) (Ref. 71) of N₂O belongs to the bending vibrational mode, as illustrated in Fig. 5(b). It can be well approximated by a two-dimensional (2D) isotropic harmonic oscillator model. The energy level for 2D isotropic harmonic oscillator is $E_j = (j + 1/2)h\nu$, and the energy degeneracy is $j + 1$. The populations at each energy level calculated using Boltzmann distributions were shown in Fig. 5(a). The potential energy curve was calculated by DFT-B3LYP method with the correlated consistent basis sets aug-cc-pVQZ.⁷² Figure 5(b) shows the potential energy curve, vibrational wave functions, and populations at each energy level. At room temperature (300 K), N₂O dominantly stays at the vibrational ground state (88.6%), and has 10.5% population at the first vibrational excited state.

To calculate the thermally averaged momentum distributions, it was assumed the electron can immediately follow the nuclear motions. If neglecting the population at the vibrational level $j > 3$, the thermally averaged momentum distribution $\rho_{av}(p)$ can be given by

$$\rho_{av}(p) = \sum_n \rho_{\theta_n}(p) \frac{\sum_{j=0}^2 (j+1) e^{-\frac{E_j}{kT}} \int_{\theta_n-\epsilon}^{\theta_n+\epsilon} 2\pi |\Phi_j(\theta)|^2 \theta d\theta}{\sum_{j=0}^2 (j+1) e^{-\frac{E_j}{kT}}}, \quad (8)$$

where $\rho_{\theta_n}(p)$ is the momentum distributions when N₂O with a bending angle θ_n , $\Phi_j(\theta)$ is j th vibrational wavefunction for the bending mode, θ is the bending angle, and T is the temperature. The population versus the bending angle θ was plotted in Fig. 6(a). It can be seen the most probable angle at room temperature is roughly 6°. As Fig. 6(b) shows, the thermally averaged momentum distributions of peak 3 slightly increase at the low momentum region when compared with that of equilibrium configuration. There is no notable difference either for other valence orbitals. Therefore, the discrepancy between the calculations and experimental results in Figs. 2(a) and 2(c) is not due to the vibrational effects. Further high level calculations with taking account of some dynamic effects may help clarify this issue.

IV. SUMMARY

In present work, Dyson orbitals of N₂O were comprehensively studied by the high resolution EMS experiment in cooperation with the bench-marked SAC-CI method. Ionization energy spectrum and momentum distributions of orbitals in both outer valence region and inner valence region can be well described by the SAC-CI General-R method. To investigate the unexpected higher intensity at low momentum region for peak 1 and peak 3, the vibrational effects on momentum distributions were investigated through the statistical average. It was found that the vibration had no visible effects on the momentum distributions of N₂O at room temperature. The discrepancy needs further investigations.

ACKNOWLEDGMENTS

This work is supported by the National Natural Science Foundation of China (Grant Nos. 11074144, 10874097 and 10704046) and Specialized Research Fund for the Doctoral Program of Higher Education (Grant No. 20070003146).

- ¹E. Weigold and I. E. McCarthy, *Electron Momentum Spectroscopy* (Kulwer Academic, New York, 1999).
- ²M. A. Coplan, J. H. Moore, and J. P. Doering, *Rev. Mod. Phys.* **66**, 985 (1994).
- ³I. E. McCarthy and E. Weigold, *Rep. Prog. Phys.* **54**, 789 (1991).
- ⁴K. T. Leung and C. E. Brion, *Chem. Phys.* **82**, 87 (1983).
- ⁵C. G. Ning, X. G. Ren, J. K. Deng, S. F. Zhang, G. L. Su, F. Huang, and G. Q. Li, *J. Chem. Phys.* **122**, 224302 (2005).
- ⁶I. V. Litvinyuk, Y. Zheng, and C. E. Brion, *Chem. Phys.* **253**, 41 (2000).
- ⁷J. Rolke, Y. Zheng, C. E. Brion, Z. Shi, S. Wolfe, and E. R. Davidson, *Chem. Phys.* **244**, 1 (1999).
- ⁸C. G. Ning, X. G. Ren, J. K. Deng, G. L. Su, Z. F. Zhang, S. Knippenberg, and M. S. Deleuze, *Chem. Phys. Lett.* **421**, 52 (2006).
- ⁹C. E. Brion, *Int. J. Quantum Chem.* **29**, 1397 (1986).
- ¹⁰H. Nakatsuji, *Chem. Phys. Lett.* **59**, 362 (1978).
- ¹¹H. Nakatsuji and K. Hirao, *Int. J. Quantum Chem.* **20**, 1301 (1981).
- ¹²S. J. Cavanagh and B. Lohmann, *J. Phys. B* **32**, L261 (1999).
- ¹³J. Lopes, V. Tarnovsky, M. Gutkin, and K. Becker, *Int. J. Mass Spectrom.* **225**, 25 (2003).
- ¹⁴B. G. Lindsay, R. Rejoub, and R. F. Stebbings, *J. Chem. Phys.* **118**, 5894 (2003).
- ¹⁵F. Biondini, B. G. Brunetti, P. Candori, F. Angelis, S. Falcinelli, F. Taranelli, F. Pirani, and F. Vecchiocattivi, *J. Chem. Phys.* **122**, 164308 (2005).
- ¹⁶G. J. Rathbone, E. D. Poliakov, J. D. Bozek, D. Toffoli, and R. R. Lucchese, *J. Chem. Phys.* **123**, 014307 (2005).
- ¹⁷K. N. Josphipura, S. Gangopadhyay, and B. G. Vaishnav, *J. Phys. B* **40**, 1953 (2007).

- ¹⁸A. L. Natalie and D. P. Stephen, *Phys. Chem. Chem. Phys.* **6**, 4558 (2004).
- ¹⁹Y. K. Kim, W. Hwang, N. M. Weinberger, M. A. Ali, and M. E. Rudd, *J. Chem. Phys.* **106**, 1026 (2005).
- ²⁰M. Ehara, M. Ishida, and H. Nakatsuji, *Collect. Czech. Chem. Commun.* **73**, 771 (2008).
- ²¹R. Gaspar and A. Nagy, *Acta Phys. Acad. Sci. Hung.* **50**, 359 (1981).
- ²²F. Wang, M. J. Brunger, and F. P. Larkins, *J. Phys. Chem. A* **105**, 1254 (2001).
- ²³R. D. Harcourt, F. Wang, and T. M. Klapotke, *J. Mol. Model.* **7**, 271 (2001).
- ²⁴F. Wang, F. P. Larkins, M. J. Brunger, M. T. Michalewicz, and D. A. Winkler, *Spectrochim. Acta, Part A* **57**, 9 (2001).
- ²⁵W. Domcke, L. S. Cederbaum, J. Schirmer, W. von Niessen, C. E. Brion, and K. H. Tan, *Chem. Phys.* **40**, 171 (1979).
- ²⁶M. Gerard, T. R. Govers, and R. Marx, *Chem. Phys.* **36**, 247 (1979).
- ²⁷D. M. P. Holland, M. A. Macdonald, and M. A. Hayes, *Chem. Phys.* **142**, 291 (1990).
- ²⁸U. Gelius, *J. Electron. Spectrosc.* **5**, 985 (1974).
- ²⁹C. E. Brion and K. H. Tan, *Chem. Phys.* **34**, 141 (1978).
- ³⁰M. Ehara, S. Yasuda, and H. Nakatsuji, *Z. Phys. Chem.* **217**, 161 (2003).
- ³¹A. Minchinton, I. Fuss, and E. Weigold, *J. Electron Spectrosc. Relat. Phenom.* **27**, 1 (1982).
- ³²R. Fantoni, A. Giardini, and R. Tiribelli, *Chem. Phys. Lett.* **71**, 335 (1980).
- ³³Y. Khajuria, M. Takahashi, and Y. Udagawa, *J. Electron Spectrosc. Relat. Phenom.* **133**, 113 (2003).
- ³⁴W. von Niesson, J. Schirmer, and L. S. Cederbaum, *Comput. Phys. Rep.* **1**, 57 (1984).
- ³⁵J. V. Ortiz, *J. Chem. Phys.* **89**, 6348 (1988).
- ³⁶X. G. Ren, C. G. Ning, J. K. Deng, S. F. Zhang, G. L. Su, F. Huang, and G. Q. Li, *Rev. Sci. Instrum.* **76**, 063103 (2005).
- ³⁷C. G. Ning, S. F. Zhang, J. K. Deng, K. Liu, Y. R. Huang, and Z. H. Luo, *Chin. Phys. B* **17**, 1729 (2008).
- ³⁸R. K. Singh, J. V. Ortiz, and M. K. Mishra, *Int. J. Quantum. Chem.* **110**, 1901 (2010).
- ³⁹C. M. Oana and A. I. Krylov, *J. Chem. Phys.* **127**, 234106 (2007).
- ⁴⁰M. Yamazaki, T. Horio, N. Kishimoto, and K. Ohno, *Phys. Rev. A* **75**, 032721 (2007).
- ⁴¹M. E. Casida and D. P. Chong, *Int. J. Quantum. Chem.* **40**, 225 (1991).
- ⁴²P. Duffy, D. P. Chong, M. E. Casida, and D. R. Salahub, *Phys. Rev. A* **50**, 4707 (1994).
- ⁴³Y. Zheng, C. E. Brion, M. J. Brunger, K. Zhao, A. M. Grisogono, S. Braidwood, E. Weigold, S. J. Chakravorty, E. R. Davidson, A. Sgamellotti, and W. von Niessen, *Chem. Phys.* **212**, 269 (1996).
- ⁴⁴H. Nakatsuji, *J. Chem. Phys.* **83**, 5743 (1985).
- ⁴⁵H. Nakatsuji, *J. Chem. Phys.* **94**, 6716 (1991).
- ⁴⁶H. Nakatsuji, *Chem. Phys. Lett.* **177**, 331 (1990).
- ⁴⁷H. Nakatsuji, *Chem. Phys. Lett.* **67**, 329 (1979).
- ⁴⁸H. Nakatsuji, O. Kitao, and T. Toneyzawa, *J. Chem. Phys.* **83**, 723 (1985).
- ⁴⁹M. Ehara, M. Ishida, and H. Nakatsuji, *J. Chem. Phys.* **114**, 8990 (2001).
- ⁵⁰M. Ehara, Y. Ohtsuka, H. Nakatsuji, M. Takahashi, and Y. Udagawa, *J. Chem. Phys.* **122**, 1 (2005).
- ⁵¹J. A. Pople, J. S. Binkley, and R. Seeger, *Int. J. Quantum Chem. Symp.* **10**, 1 (1976).
- ⁵²J. A. Pople, R. Seeger, and R. Krishnan, *Int. J. Quantum Chem. Symp.* **12**, 149 (1977).
- ⁵³M. F. Frisch, G. W. Trucks, H. B. Schlegel *et al.*, GAUSSIAN 03, Revision E.01, Gaussian Inc., Wallingford CT, 2004.
- ⁵⁴C. G. Ning, B. Hajgató, Y. R. Huang, S. F. Zhang, K. Liu, Z. H. Luo, S. Knippenberg, J. K. Deng, and M. S. Deleuze, *Chem. Phys.* **343**, 19 (2008).
- ⁵⁵D. P. Chong, O. V. Gritsenko, and E. J. Baerends, *J. Chem. Phys.* **116**, 1760 (2002).
- ⁵⁶A. D. Becke, *J. Chem. Phys.* **98**, 5648 (1993).
- ⁵⁷C. Lee, W. Yang, and R. G. Parr, *Phys. Rev. B* **37**, 785 (1988).
- ⁵⁸P. Hohenberg and W. Kohn, *Phys. Rev.* **136**, B864 (1964).
- ⁵⁹S. H. Vosko, L. Wilk, and M. Nusair, *Can. J. Phys.* **58**, 1200 (1980).
- ⁶⁰J. P. Perdew, K. Burke, and M. Ernzerhof, *Phys. Rev. Lett.* **78**, 1396 (1997).
- ⁶¹E. R. Davidson, *Chem. Phys. Lett.* **220**, 514 (1996).
- ⁶²C. G. Ning, X. G. Ren, J. K. Deng, G. L. Su, S. F. Zhang, and G. Q. Li, *Phys. Rev. A* **73**, 022704 (2006).
- ⁶³X. G. Ren, C. G. Ning, J. K. Deng, S. F. Zhang, G. L. Su, F. Huang, and G. Q. Li, *Phys. Rev. Lett.* **94**, 163201 (2005).
- ⁶⁴C. G. Ning, Z. H. Luo, Y. R. Huang, B. Hajgató, F. Morini, K. Liu, S. F. Zhang, J. K. Deng, and M. S. Deleuze, *J. Phys. B* **41**, 175103 (2008).
- ⁶⁵Z. H. Luo, C. G. Ning, K. Liu, Y. R. Huang, and J. K. Deng, *J. Phys. B* **42**, 165205 (2009).
- ⁶⁶M. S. Deleuze, W. N. Pang, A. Salam, and R. C. Shang, *J. Am. Chem. Soc.* **123**, 4049 (2001).
- ⁶⁷S. Knippenberg, Y. R. Huang, B. Hajgató, J. P. Francois, J. K. Deng, and M. S. Deleuze, *J. Chem. Phys.* **127**, 174306 (2007).
- ⁶⁸C. G. Ning, Y. R. Huang, S. F. Zhang, J. K. Deng, K. Liu, Z. H. Luo, and F. Wang, *J. Phys. Chem. A* **112**, 11078 (2008).
- ⁶⁹F. Morini, S. Knippenberg, M. S. Deleuze, and B. Hajgató, *J. Phys. Chem. A* **114**, 4400 (2010).
- ⁷⁰K. Liu, C. G. Ning, Z. H. Luo, L. L. Shi, and J. K. Deng, *Chem. Phys. Lett.* **497**, 229 (2010).
- ⁷¹G. Herzberg, *Molecular Spectra and Molecular Structure (I Spectra of Diatomic Molecules)* (D. Van Nostrand, New York, 1953).
- ⁷²D. E. Woon and T. H. Dunning, Jr., *J. Chem. Phys.* **98**, 1358 (1993).
- ⁷³G. Velde, F. M. Bickelhaupt, E. J. Baerends, C. F. Guerra, S. J. A. VAN Gisbergen, J. G. Snijders, and T. Ziegler, *J. Comput. Chem.* **22**, 931 (2001).